known distance (125 pc), and temperature (16 K), Barnard 68 has a physical radius of 12,500 AU, a mass of 2.1 solar masses, and a pressure at its boundary of $P = 2.5 \times 10^{-12}$ Pa. This surface pressure is an order of magnitude higher than that of the general interstellar medium[22] but it is in rough agreement with the pressure inferred for the Loop I superbubble from X-ray observations with the ROSAT satellite[13]. The close correspondence of the observed extinction profile with that predicted for a Bonnor–Ebert sphere strongly suggests that Barnard 68 is indeed an isothermal, pressure-confined and self-gravitating cloud. It is also likely to be in a state near hydrostatic equilibrium with thermal pressure primarily supporting the cloud against gravitational contraction.

For Barnard 68, $\xi_{max}$ is very near and slightly in excess of the critical radial parameter and the cloud may be only marginally stable and on the verge of collapse. However, in the likely case that the cloud contains a static magnetic field[23–25], the additional internal magnetic pressure can act to stabilize it at a density contrast slightly higher than that predicted by the Bonnor–Ebert theory. Nevertheless, inevitable physical processes, such as cloud cooling, the natural reduction of internal magnetic flux by ambipolar diffusion[26,27], as well as any increase in external pressure, will readily destabilize the Barnard 68 cloud and result in the formation of a low-mass star, similar to the Sun.

Finally, we suggest that Barnard 68, and its neighbouring globules B69, B70 and B72 may be the precursor of an isolated and sparsely populated association of young low-mass stars similar to the recently identified TW Hydra[28] association. The TW Hydra association is a stellar group near the solar system consisting of a handful of young low-mass, Sun-like stars. The existence of such a young stellar group presents an interesting problem to astronomers because its origin is difficult to explain given its youth and relatively large distance from known sites of star formation. Bok globules such as those in the Barnard 68 group are thought to be remnant dense cores produced as a result of the interaction of massive O stars and molecular clouds[29]. Over their short lifetimes such massive stars, through ionization, stellar winds and ultimately supernova explosions, very effectively disrupt the molecular clouds from which they formed. In the process large shells of expanding gas are created. When surrounding clouds are disrupted by the passage of these shells, a few of their most resilient dense cores will be left behind, embedded within the shell's hot interior. Remnant cores with just the right mass can establish pressure equilibrium with the hot gas within the shell and survive to become Bok globules. Eventually, as a result of the processes described above, these clouds will evolve to form low-mass, Sun-like stars which are relatively isolated and far from the original birthplace of the O stars. Up to 35% of all Bok globules contain newly formed stars[30] and thus it is likely that our observations of the starless Barnard 68 cloud provide the first detailed description of the initial conditions which exist before the collapse of dark globules and the formation of isolated, low-mass stars. □

Received 19 September; accepted 3 November 2000.


1. Ebert, R. Uber die Verdichtung von HI-Gebieten. *Z. Astrophys.* **37,** 217–232 (1955).
2. Bonnor, W. Boyle's Law and gravitational instability. *Mon. Not. R. Astron. Soc.* **116,** 351–359 (1956).
3. Alves, J., Lada, C. & Lada, E. Correlation between gas and dust in molecular clouds: L977. *Astrophys. J.* **515,** 265–274 (1999).
4. Chandler, C. & Richer, J. The structure of protostellar envelopes derived from submillimeter continuum images. *Astrophys. J.* **350,** 851–866 (2000).
5. Lada, C., Lada, E., Bally, J. & Clemens, D. Dust extinction and molecular gas in the dark cloud IC 5146. *Astrophys. J.* **429,** 694–709 (1994).
6. Alves, J., Lada, C. J., Lada, E. A., Kenyon, S. J. & Phelps, R. Dust extinction and molecular cloud structure: L 977. *Astrophys. J.* **506,** 292–305 (1998).
7. Lada, C., Alves, J. & Lada, E. Infrared extinction and the structure of the IC 5146 dark cloud. *Astrophys. J.* **512,** 250–259 (1999).
8. Bok, B. & Reilly, E. Small dark nebulae. *Astrophys. J.* **105,** 255–257 (1947).
9. Clemens, D. & Barvainis, R. A catalog of small, optically selected molecular clouds: optical, infrared, and millimeter properties. *Astrophys. J. Suppl. Ser.* **68,** 257–286 (1988).
10. de Geus, E., de Zeeuw, P. & Lub, J. Physical parameters of stars in the Scorpius-Centaurus OB association. *Astron. Astrophys.* **216,** 44–61 (1989).
11. Bourke, T., Hyland, A., Robinson, G., James, S. & Wright, C. Studies of star formation in isolated small dark clouds—II A southern ammonia survey. *Mon. Not. R. Astron. Soc.* **276,** 1067–1084 (1995).
12. Quigley, M. & Haslam, C. Structure of the radio continuum background at high galactic latitudes. *Nature* **208,** 741–743 (1965).
13. Breitschwerdt, D., Freyberg, M. & Egger, R. Origin of H I clouds in the local bubble. *Astron. Astrophys.* **361,** 303–320 (2000).
14. Reipurth, B., Nyman, L. & Chini, R. Protostellar candidates in southern molecular clouds. *Astron. Astrophys.* **314,** 258–264 (1996).
15. Moorwood, A., Cuby, J. & Lidman, C. SOFI sees first light at the NTT. *ESO Messenger* **91,** 9–13 (1998).
16. Appenzeller, I. *et al.* Successful commissioning of FORSI—the first optical instrument on the VLT. *ESO Messenger* **94,** 1–6 (1998).
17. Mathis, J. Interstellar dust and extinction. *Annu. Rev. Astron. Astrophys.* **28,** 37–70 (1990).
18. Bok, B. *Centennial Symposia* (Harvard Observatory Monographs No. 7, Harvard-College Observatory, Cambridge, 1948).
19. Lane, J. *Am. J. Sci. Arts, Series 2* **4,** 57 (1870).
20. Emden, R. *Gaskugeln* (Teubner, Leipzig, 1907).
21. Chandrasekhar, S. in *An Introduction to the Study of Stellar Structure* 156 (Dover, Toronto, 1967).
22. Mckee, C. in *The Origin of Stars and Planetary Systems* (eds Lada, C. & Kylafis, N.) 29–66 (Kluwer, Dordrecht, 1999).
23. Nakano, T. Quasistatic contraction of magnetic protostars due to magnetic flux leakage—Part One—formulation and an example. *Publ. Astron. Soc. Jpn* **31,** 697–712 (1979).
24. Lizano, S. & Shu, F. Molecular cloud cores and bimodal star formation. *Astrophys. J.* **342,** 834–854 (1989).
25. Basu, S. & Mouschovias, T. Magnetic braking, ambipolar diffusion, and the formation of cloud cores and protostars I—Axisymmetric solutions. *Astrophys. J.* **432,** 720–741 (1994).
26. Shu, F., Allen, A., Shang, H., Ostriker, E. & Li, Z. in *The Origin of Stars and Planetary Systems* (eds Lada, C. & Kylafis, N.) 193–226 (Kluwer, Dordrecht, 1999).
27. Mouschovias, T. & Ciolek, G. in *The Origin of Stars and Planetary Systems* (eds Lada, C. & Kylafis, N.) 305–340 (Kluwer, Dordrecht, 1999).
28. Rucinski, S. & Krautter, J. TW Hya: a T Tauri star far from any dark cloud. *Astron. Astrophys.* **121,** 217–225 (1983).
29. Reipurth, B. Star formation in Bok globules and low-mass clouds. I—The cometary globules in the Gum Nebula. *Astron. Astrophys.* **117,** 183–198 (1983).
30. Launhardt, R. & Henning, T. Millimetre dust emission from northern Bok globules. *Astron. Astrophys.* **326,** 329–346 (1997).



### Acknowledgements

We thank M. Lombardi for fruitful discussions and assistance, the Paranal Science Operations team for observing Barnard 68 with FORS1 on Very Large Telescope (VLT) Antu, R. West and E. Janssen for composing Figure 1 top, and R. Hook and R. Fosbury for composing Figure 1 bottom. We also thank M. Petr for helpful discussions during the preparation of the VLT observations. E.A.L. acknowledges support from a Presidential Early Career Award for Scientists and Engineers to the University of Florida.


Correspondence and requests for materials should be addressed to J.A. (e-mail: jalves@eso.org).

# Quantum metallicity in a two-dimensional insulator

**V. Yu. Butko*† & P. W. Adams***

** Department of Physics and Astronomy, Louisiana State University, Baton Rouge, Louisiana 70803, USA*
*† Ioffe Physical Technical Institute (PTI), Russian Academy of Sciences, Polytekhnicheskaya Street, 26, 194021, St Petersburg, Russia*

**One of the most far-reaching problems in condensed-matter physics is to understand how interactions between electrons, and the resulting correlations, affect the electronic properties of disordered two-dimensional systems. Extensive experimental[1–6] and theoretical[7–11] studies have shown that interaction effects are enhanced by disorder, and that this generally results in a depletion of the density of electronic states. In the limit of strong disorder, this depletion takes the form of a complete gap[12,13] in the density of states. It is known that this 'Coulomb gap' can turn a pure metal film that is highly disordered into a poorly conducting insulator[14], but the properties of these insulators are not well understood. Here we investigate the electronic properties of disordered beryllium films, with the aim of disentangling the effects of the Coulomb gap and the underlying disorder. We show that the gap is suppressed by a magnetic field and that this drives**

**the strongly insulating beryllium films into a low-temperature 'quantum metal' phase with resistance near the quantum resistance $R_Q = h/e^2$, where $h$ is Planck's constant and $e$ is the electron charge.**

The theory of interaction effects in disordered electronic systems has for the most part been developed for two extreme limits. In the two-dimensional (2D) weak disorder limit in which the film resistance $R$ is much less than $R_Q = 26\,k\Omega$, electron–electron (e–e) interactions produce an anomalous logarithmic suppression of the density of states (DOS) at the Fermi energy[9,15,16]. These interactions also, along with coherent backscattering[4,7], produce a weak logarithmic increase in $R$ with decreasing temperature, which is commonly referred to as weak localization. We will refer to metal films in this limit as being 'weakly metallic' because the observed increases in $R$ with decreasing temperature are typically of the order of a few per cent. In the opposite limit, that is, the strongly insulating regime, the e–e interactions grow rapidly and ultimately produce the Coulomb gap in the DOS[12]. The 2D gap spectrum is predicted to be linear in energy[12], and, in contrast to the weak localization regime, it completely dominates the transport behaviour of the system and can produce many orders of magnitude increases in $R$ with decreasing temperature.

We chose to fabricate our metal films using beryllium, because it is known to form a smooth, dense, non-granular morphology when thermally evaporated onto glass[17]. This morphology is crucial in that it ensures that the measured resistance is representative of e–e correlation effects and not grain charging effects. In the present study we used films with thicknesses of ~1.7 nm and corresponding low-temperature sheet resistances in the range $3R_Q$–$5R_Q$. They were deposited by thermally evaporating 99.5% pure beryllium metal onto fire-polished glass substrates held at 84 K. The evaporations were performed in a $4 \times 10^{-7}$ torr vacuum at a rate of ~0.15 nm $s^{-1}$. The film area was 1.5 mm × 4.5 mm. The tunnel junctions were formed by exposing the films to the atmosphere for 0.1–3 h in order to form a native oxide. Then a 20-nm-thick Ag counter-electrode was deposited directly on top of the film, with the oxide serving as the tunnel barrier; the junction area was 0.7 mm × 0.7 mm. The resistance of all of the samples discussed below was high enough to suppress completely the superconducting phase. The film resistances were measured using a standard four-probe a.c. current–voltage ($I$–$V$) technique, and the tunnelling conductances were measured using a d.c. technique. Magnetoresistance (MR) measurements were made with the magnetic field oriented perpendicular to the film surface.

In Fig. 1 we plot the temperature dependence of the film resistance (normalized by $R_Q$) for two critically disordered samples; the resistance of each film was measured in zero field and in a field of 8.4 T. The zero-field data are strongly insulating, but the high-field data appear to be more metallic in character: the magnetic field is producing a significant suppression of the insulating phase. This is also evident in Fig. 2, where we show the low-temperature MR of the films. We note that the low-field MR is positive, but above 1 T the MR becomes strongly negative. Similar behaviour has recently been reported in much higher-resistance Be films, $R \approx 100R_Q$, which obeyed the Efros–Shklovskii hopping law[12,14,18], $R = (R_Q/2)\exp(T_o/T)^{1/2}$, where $T_o$ is the correlation energy and $T$ is the temperature. These extremely insulating films exhibited a small, positive MR at low field, followed by a tenfold negative MR with no signs of saturation up to ~9 T. The negative MR was well described by a $1/R \propto H$ dependence[18] (where $H$ is the magnetic

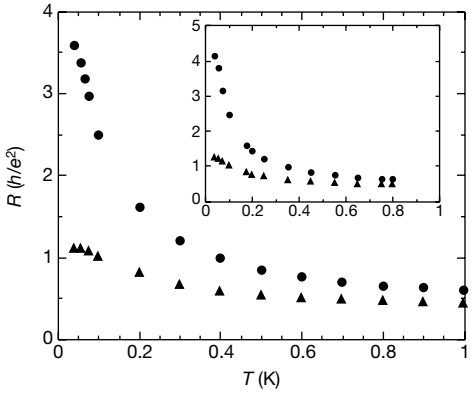


**Figure 1** Temperature dependence. The figure shows the resistance of film B57 in units of $h/e^2$ in zero field (circles) and at a perpendicular magnetic field of $H = 8.4$ T (triangles) as a function of temperature. Inset, temperature dependence of the resistance of sample B55.

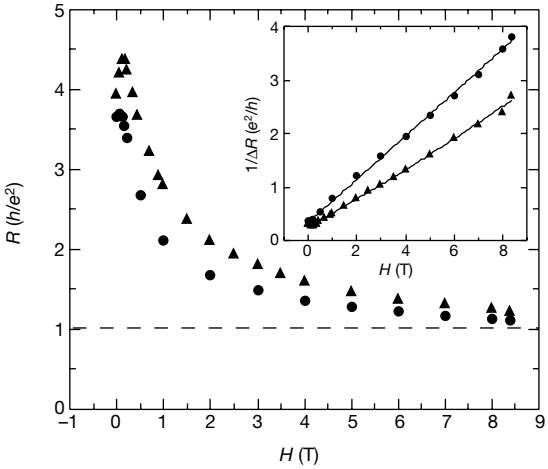


**Figure 2** Low-temperature magnetoresistance. The figure shows the resistance in units of $h/e^2$ as a function of magnetic field $H$ at $T = 40$ mK, for samples B57 (circles) and B55 (triangles). We note the saturation at $R \approx h/e^2$. Inset, linear behaviour after subtracting a saturation resistance of 0.85 $h/e^2$, $\Delta R = R - 0.85$. The solid lines are guides to the eye.

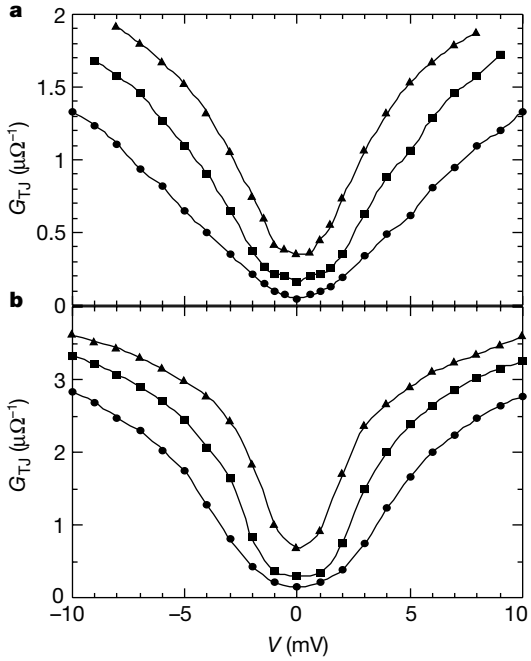


**Figure 3** Tunnelling density of states. **a**, Low-temperature tunnelling conductance ($G_{TJ}$) of the B55 film at $H = 0$ (circles), $H = 3.0$ T (squares) and $H = 8.4$ T (triangles). **b**, As **a** but for the B57 film. The tunnelling conductance is proportional to the density of electronic states which clearly increases with increasing field. The solid lines are guides to the eye.

field intensity) which was shown to arise from a field suppression of the correlation energy $T_o$, suggesting that the Coulomb gap itself is field-dependent. The overall structure of the data in Fig. 2 is consistent with the MR behaviour of the highly insulating films of ref. 18, with the notable exception of the saturation of the MR to the quantum resistance.

The saturation behaviour in Fig. 2 suggests that the film resistance can be written as the sum of two terms:

$$R = R_{ee} + \beta R_Q \quad (1)$$

where $R_{ee}$ is a field-dependent correlation resistance and the second term is a field-independent background. The constant $\beta$ is only weakly temperature-dependent, and is of order unity. If we take $\beta = 0.85$ and subtract the background resistance from the MR data, then we find that $1/R_{ee} \propto H$, as shown in the inset of Fig. 2. This is precisely the field dependence reported in the $R \approx 100R_Q$ Be films of ref. 18, suggesting that the negative MR of those films would have also saturated to the quantum resistance at $H \approx 100$ T. Indeed, a compelling interpretation of the data in Figs 1 and 2 is that the field drives the system out of an insulating phase, which is dominated by $R_{ee}$ into a weakly metallic phase at a universal quantum resistance. We have termed this high-field phase a 'quantum metal' by virtue of its extremely weak temperature dependence and the fact that its resistance is near the quantum resistance $R_Q$. In terms of the MR measurements of films of ref. 18, the quantum metal phase would have been reached at a field high enough to drive $T_o$ to zero.

The correlation resistance $R_{ee}$ and its field dependence manifest the physical processes that are also associated with the emergence of the Coulomb gap. In Fig. 3 we plot the tunnelling conductance as a function of bias voltage at several field values for both samples. At low temperatures, the tunnelling conductance is proportional to the electronic DOS of the films[19] with $V = 0$ corresponding to the Fermi energy. We note that the zero-field curves in Fig. 3 show an almost complete depletion of states in the vicinity of $V = 0$. This is consistent with the linear Coulomb gap spectra reported in studies of much higher-resistance Be films in ref. 14. The most interesting aspect of Fig. 3, however, is that the application of field causes a significant increase in the number of states near the Fermi energy[20] with a corresponding decrease in film resistance.

We believe that the field dependence of the DOS spectrum is reflected in the field dependence of $R_{ee}$ and that $R_{ee} \rightarrow 0$ in the limit of $H \rightarrow \infty$. The quantum resistance emerges once the gap is lifted by the field. We point out here that the saturation of the MR in Fig. 2 is not reflected in the DOS field dependence. In Fig. 4 we plot the relative tunnelling conductance at zero bias (that is, the Fermi energy) as a function of field. These data clearly show that the number of excess states is proportional to the field with no sign of saturation up to 9 T, though the MR does saturate in this field range.

The low-temperature magnetotransport characteristics of the Be films are most effectively summarized using the schematic phase diagram in Fig. 5. The $x$ axis measures the amount of disorder, which we parametrize as $1/t$ where $t$ is the film thickness. The $y$ axis is the applied magnetic field. In the limit of $1/t \rightarrow 0$ the films are three-dimensional (3D) and have finite resistance at zero temperature. As the thickness is lowered, however, the 3D to 2D threshold is crossed, and the films become weakly metallic with a perturbative logarithmic increase in resistance with decreasing temperature and a perturbative logarithmic suppression of the DOS near the Fermi energy. We note that Be also has a locally enhanced superconducting phase in the weakly metallic regime, shown in blue in Fig. 5 (The bulk superconducting transition temperature of Be is $T_c = 26$ mK: at $t \approx 5$ nm, the film resistance is $R \approx 0.1$ kΩ and $T_c \approx 0.6$ K; at $t \approx 1.8$ nm, $R \approx 10$ kΩ and $T_c \approx 0$). As the film thickness is further decreased in zero field the resistance increases. When $R \approx R_Q$ the depletion of states near the Fermi energy grows exponentially[14] with increasing $R$, signalling the emergence of the Coulomb gap. This crossover is depicted by the green-yellow hatched boundary between the weakly and strongly correlated regions in the diagram. Further decreases in thickness at zero field result in films with $R \gg R_Q$. These films are correlated insulators, shown in red, and are characterized by a well defined Coulomb gap and Efros–Shklovskii hopping transport. The further one moves to the right in the correlated insulator region of the diagram the greater the correlation energy $T_o$ becomes, until one eventually reaches the percolation threshold of the film, at which point it is no longer electrically continuous. This occurs at $t \approx 1$ nm in Be films. We have shown that the application of a magnetic field lifts the Coulomb gap, thereby producing extremely large decreases in resistance at low temperatures. As the diagram in Fig. 5 indicates, we believe that this process eventually leads to a saturation in the resistance near $R_Q$ even for films deep in the correlated insulator regime. This weakly temperature-dependent, high-field state is depicted in yellow and essentially behaves as a weak metal. Thus the yellow region in Fig. 5 describes films of varying disorder but with resistance near $R_Q$. The almost ideal morphological characteristics of Be films, along with the fact that Be is intrinsically non-magnetic, lead us to believe that the general features of Fig. 5 are generic to high-density, disordered, 2D electron gases. □

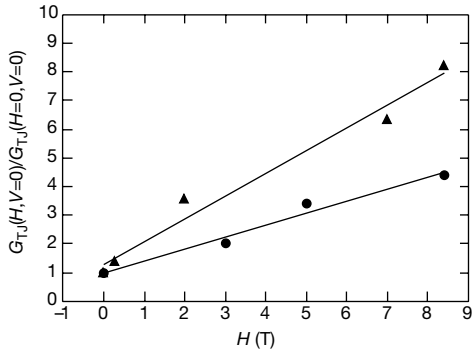


**Figure 4** Zero-bias tunnelling conductance. The figure shows relative zero-bias tunnelling conductance as a function of magnetic field at $T = 100$ mK for samples B55 (triangles) and B57 (circles). The solid lines are guides to the eye.

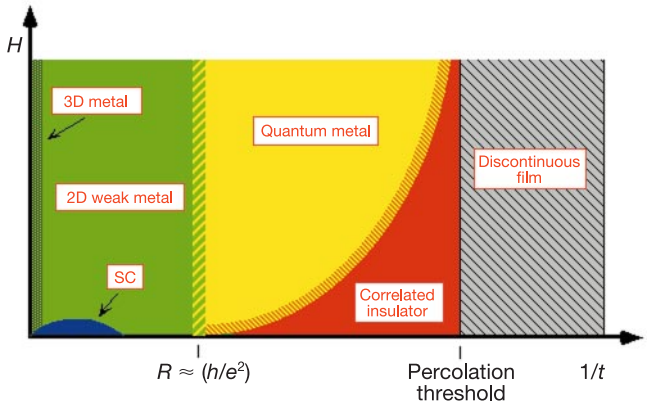


**Figure 5** Phase diagram. The figure shows the low-temperature electronic phase diagram of Be films where $H$ is the magnetic field intensity and $t$ is the film thickness. We interpret $1/t$ as a disorder parameter.

Received 24 July; accepted 9 November 2000.

1. Hsu, S.-Y. & Valles, J. M. Jr Electron tunneling into strongly disordered films: the influence of structure on e-e interactions. *Phys. Rev. B* **49,** 16600–16604 (1994).
2. Vaknin, A., Ovadyahu, Z. & Pollak, M. Evidence for interactions in nonergodic electronic transport. *Phys. Rev. Lett.* **81,** 669–672 (1998).
3. Nissim, M., Leareah, Y. & Rosenbaum, R. Dominating Coulomb-interaction effects in amorphous $In_xO_y$ films. *Phys. Rev. B* **40,** 6351–6355 (1989).
4. Bishop, D. J., Dynes, R. C. & Tsui, D. C. Magnetoresistance in Si metal-oxide-semiconductor field-effect transistors: Evidence of weak localization and correlation. *Phys. Rev. B* **26,** 773–779 (1982).

5. Das Sarma, S. & Pinczuk, A. (eds) *Perspectives in Quantum Hall Effects* (Wiley, New York, 1997).
6. Kravchenko, S. V., Kravchenko, G. V., Furneaux, J. E., Pudalov, V. M. & D'Iorio, M. Possible metal-insulator transition at B = 0 in two dimensions. *Phys. Rev. B* **50,** 8039–8042 (1994).
7. Lee, P. A. & Ramakrishnan, T. V. Disordered electronic systems. *Rev. Mod. Phys.* **57,** 287–337 (1985).
8. Ando, T., Fowler, A. B. & Stern, F. Electronic properties of two-dimensional systems. *Rev. Mod. Phys.* **54,** 437–672 (1982).
9. Altshuler, B. L., Aronov, A. G., Gershenson, M. E. & Sharvin, Yu. V. Quantum effects in disordered metal films. *Sov. Sci. Rev. A Phys.* **9,** 223–353 (1987).
10. Belitz, D. & Kirkpatrick, T. R. The Anderson-Mott transition. *Rev. Mod. Phys.* **66,** 261–390 (1994).
11. Pastor, A. A. & Dobrosavljevic, V. Melting of the electron gas. *Phys. Rev. Lett.* **83,** 4642–4645 (1999).
12. Shklovskii, B. I. & Efros, A. L. *Electronic Properties of Doped Semiconductors* (Springer, New York, 1984).
13. Massey, J. G. & Lee, M. Electron tunneling study of Coulomb correlations across the metal-insulator transition in Si:B. *Phys. Rev. Lett.* **77,** 3399–3402 (1996).
14. Butko, V. Yu., DiTusa, J. F. & Adams, P. W. Coulomb gap: How a metal film becomes an insulator. *Phys. Rev. Lett.* **84,** 1543–1546 (2000).
15. Gershenzon, M. E., Gubankov, V. N. & Falei, M. I. Effect of electron-electron interaction on state density in 2D Al films. *Pis'ma Zh. Eksp. Teor. Fiz.* **41,** 435–439 (1985) [*JETP Lett.* **41,** 535–538 (1985)].
16. Imry, Y. & Ovadyahu, Z. Density of states anomalies in disordered metal films. *Phys. Rev. Lett.* **49,** 841–844 (1982).
17. Adams, P. W., Herron, P. & Meletis, E. I. First-order spin-paramagnetic transition and tri-critical point in ultrathin Be films. *Phys. Rev. B* **58,** 2952–2955 (1998).
18. Butko, V. Yu., DiTusa, J. F. & Adams, P. W. Tenfold magnetoconductance in a non-magnetic metal film. *Phys. Rev. Lett.* **85,** 162–165 (2000).
19. Tinkam, M. *Introduction to Superconductivity* (McGraw-Hill, New York, 1996).
20. Sood, B. R. Magnetic-field-dependent zero-bias anomaly in Al-oxide-Ga (granular) thin-film tunnel junctions. *Phys. Rev. B* **25,** 6064–6066 (1982).



**Acknowledgements**

We thank J. DiTusa, D. Browne, B. Shklovskii, V. Dobrosavljevic, I. Aleiner and B. Altshuler for discussions. This work was supported by the NSF.



Correspondence and requests for materials should be addressed to P.W.A. (e-mail: adams@rouge.phys.lsu.edu).


# The relationship between fragility, configurational entropy and the potential energy landscape of glass-forming liquids


**Srikanth Sastry**

*Jawaharlal Nehru Centre for Advanced Scientific Research, Jakkur Campus, Bangalore 560064, India*



**Glass is a microscopically disordered, solid form of matter that results when a fluid is cooled or compressed in such a manner that it does not crystallize. Almost all types of materials are capable of glass formation, including polymers, metal alloys and molten salts. Given such diversity, general principles by which different glass-forming materials can be systematically classified are invaluable. One such principle is the classification of glass-formers according to their fragility[1]. Fragility measures the rapidity with which a liquid's properties (such as viscosity) change as the glassy state is approached. Although the relationship between the fragility, configurational entropy and features of the energy landscape (the complicated dependence of energy on configuration) of a glass-former have been analysed previously[2], a detailed understanding of the origins of fragility is lacking. Here I use simulations to analyse the relationship between fragility and quantitative measures of the energy landscape for a model liquid whose fragility depends on its bulk density. The results reveal that fragility depends on changes in the vibrational properties of individual energy minima in addition to their total number and spread in energy. A thermodynamic expression for fragility is derived, which is in quantitative agreement with kinetic fragilities obtained from the liquid's diffusivity.**


Glass-forming liquids grow increasingly viscous upon cooling, till the viscosity becomes so large that they fail to flow on experimental timescales. While remaining microscopically disordered like a liquid, they manifest mechanical properties of a solid; that is, they transform to a glass. By convention, the glass transition temperature $T_g$ is where the viscosity reaches a value of $10^{12}$ Pa s. The approach to this large viscosity, however, differs from one liquid to another. When displayed in an Arrhenius plot of log(viscosity) versus inverse temperature $1/T$, some liquids (such as silica) show a steady, linear increase, while others display a much steeper dependence on $1/T$ (refs 1, 3), as illustrated in Fig. 1a (inset). The former are 'strong' liquids, and the latter, 'fragile'. This range of behaviour is implicit in the Vogel–Fulcher–Tammann–Hesse (VFT) form, observed to describe the $T$ dependence of viscosity (as well as diffusivity and relaxation times) in many glass-formers. The VFT relation may be written as:

$$\eta = \eta_0 \exp\left[\frac{1}{K_{\mathrm{VFT}}(T/T_0 - 1)}\right] \qquad (1)$$

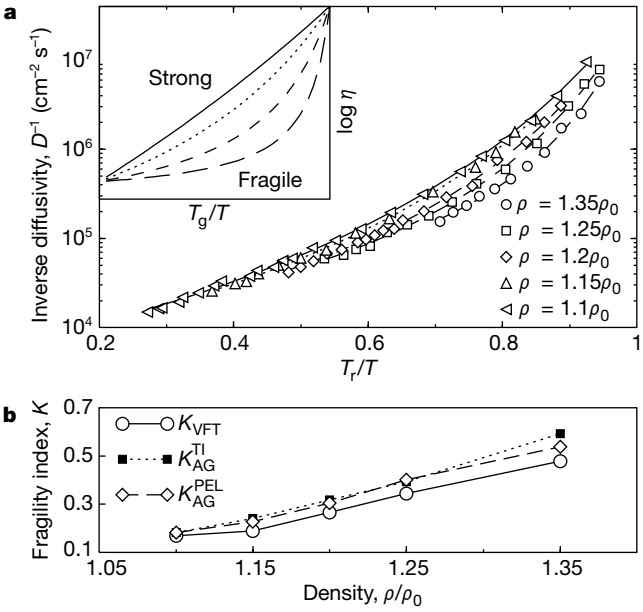


**Figure 1** Fragility plot of diffusivities, and kinetic and thermodynamic fragility indices. Results shown are obtained from molecular dynamics simulations of 204 A-type and 52 B-type particles interacting via the Lennard–Jones (LJ) potential. Argon units are used for A-type particles: LJ parameter $\epsilon_{AA} = k_B \times 119.8$ K, $\sigma_{AA} = 0.3405 \times 10^{-9} m$, $m_A = 6.6337 \times 10^{-26}$ kg; and $\epsilon_{AB}/\epsilon_{AA} = 1.5$, $\epsilon_{BB}/\epsilon_{AA} = 0.5$, $\sigma_{AB}/\sigma_{AA} = 0.8$, and $\sigma_{BB}/\sigma_{AA} = 0.88$, $m_B/m_A = 1$. Densities are reported in units of $\rho_0 = 2.53 \times 10^{28}$ m$^{-3}$ or 1.678 g cm$^{-3}$. The liquid–gas critical point is located roughly at $T_c = 130$ K, $\rho_c = 0.416\rho_0$. **a**, Diffusivities $D$ from molecular dynamics simulations (details of the simulations are as in ref. 10) are displayed in a 'fragility plot' for five densities. The reference temperature $T_r$ is chosen such that $D(T_r) = 2.44 \times 10^{-8}$ cm$^2$ s$^{-1}$, which is slightly below the lowest $D$ values measured. The VFT extrapolation is used to locate $T_r$. Fitting values $D_0$ (preexponent) are in the range of 0.87 to $2.0 \times 10^{-4}$ cm$^2$ s$^{-1}$, close to the experimentally observed values. **b**, Fragility index $K$ obtained (1) from VFT fits to diffusivities $D$; and from the configurational entropy obtained (2) from thermodynamic integration (TI), and (3) from analysis of the potential energy landscape (PEL). Dimensionless thermodynamic fragility indices are obtained by dividing $K_{AG}^{TI}$, $K_{AG}^{PEL}$ by $N\epsilon_{AA}$. Comparison with data in ref. 11 shows that at the low-density end, the fragility of the model liquid compares with that of considerably fragile liquids such as toluene, orthoterphenyl and salol, while at the high-density end, the fragility is extremely high. Temperatures of vanishing diffusivity $T_0$ from VFT fits are 18.76 K, 24.98 K, 35.97 K, 47.86 K and 75.75 K for $\rho/\rho_0 = 1.1$, 1.15, 1.2, 1.25 and 1.35 respectively.